HHS Public Access

Author manuscript

Biomaterials. Author manuscript; available in PMC 2017 December 01.

Published in final edited form as:

Biomaterials. 2016 December ; 109: 69–77. doi:10.1016/j.biomaterials.2016.09.013.

Targeted Multimodal Nano-Reporters for Pre-Procedural MRI and Intra-Operative Image-Guidance

Joonseok Lee[1], **Andrew C. Gordon**[2,6], **Hacksung Kim**[3], **Wooram Park**[2], **Soojeong Cho**[2], **Byeongdu Lee**[4], **Andrew C. Larson**[2,5,6,7,8], **Elena A. Rozhkova**[1,*], and **Dong-Hyun Kim**[2,5,*]

[1]Center for Nanoscale Materials, Argonne National Laboratory, Argonne, IL 60439, USA

[2]Department of Radiology, Northwestern University Feinberg School of Medicine, Chicago, IL 60611, USA

[3]Department of Chemistry, Northwestern University, Evanston, IL 60208, USA

[4]Advanced Photon Source, Argonne National Laboratory, Argonne, Illinois 60439, USA

[5]Robert H. Lurie Comprehensive Cancer Center, Chicago, IL 60611, USA

[6]Department of Biomedical Engineering, Northwestern University, Evanston, IL 60208, USA

[7]Department of Electrical Engineering and Computer Science, Evanston, IL 60208, USA

[8]International Institute of Nanotechnology (IIN), Northwestern University, Evanston, IL 60208, USA

Abstract

Multimodal-imaging probes offer a novel approach, which can provide detail diagnostic information for the planning of image-guided therapies in clinical practice. Here we report targeted multimodal Nd^{3+}-doped upconversion nanoparticle (UCNP) imaging reporters, integrating both magnetic resonance imaging (MRI) and real-time upconversion luminescence imaging (UCL) capabilities within a single platform. Nd^{3+}-doped UCNPs were synthesized as a core–shell structure showing a bright visible emission upon excitation at the near infrared (minimizing biological overheating and increasing tissue penetration depth) as well as providing strong MRI T2 contrast (high r_2/r_1 ratio). Transcatheter intra-arterial infusion of Nd^{3+}-doped UCNPs conjugated with anti-CD44-monoclonal antibody allowed for high performance *in vivo* multimodal UCL and MR imaging of hepatocellular carcinoma (HCC) in an orthotopic rat model. The resulted *in vivo* multimodal imaging of Nd^{3+} doped core-shell UCNPs combined with transcatheter intra-arterial targeting approaches successfully discriminated liver tumors from normal hepatic tissues in rats for surgical resection applications. The demonstrated multimodal UCL and MRI imaging capabilities of our multimodal UCNPs reporters suggest strong potential for *in vivo* visualization of tumors and precise surgical guidance to fill the gap between pre-procedural imaging and intraoperative reality.

* Corresponding author: Elena A. Rozhkova (rozhkova@anl.gov) and Dong-Hyun Kim (dhkim@northwestern.edu).

Keywords

upconversion nanoparticles; medical imaging; cancer; interventional radiology; multimodal probe

1. Introduction

Cancer is a major public health issue worldwide. Cancer comprises hundreds of distinct molecular diseases; various types of solid tumors can develop at different sites within the human body. Such broad disease profile has prompted the tailoring of cancer therapy to individual patient. Medical imaging has been playing a critical role in optimizing therapeutic strategies with early tumor detection, staging, treatment planning, and monitoring of therapeutic responses.[1, 2] Recently, innovative non-invasive imaging techniques have been developed to improve outcomes following chemotherapy or loco-regional/percutaneous ablation techniques for the treatment of cancers.[3, 4] However, surgical resection approaches that serve as the primary curative intervention for cancer remain most commonly performed under simple visual inspection and/or palpation of the interrogated tissues.[5] In many instances, ultrasonography or intraoperative magnetic resonance imaging (MRI)/ computed tomography (CT) imaging can be used to guide surgical resection but the systems may not be usable for real-time navigation, because of their prohibitive cost, large hardware footprint and use of hazardous ionizing radiation.[6, 7] Over the past years, near-infrared (NIR) fluorescent imaging has been proposed to perform pre-operative detection of lesions and for intraoperative guidance for surgery.[8, 9] NIR fluorescent organic dyes have provided real-time navigation for sentinel lymph node imaging, hepatic micrometastases detection, and surgical guidance.[8, 10] However, fundamental limitations of prior fluorescent imaging approaches in the surgical setting involve poor specificity and irreversible photochemical bleaching of injected dyes.

Upconversion luminescence (UCL) imaging using upconversion nanoparticles (UCNPs) is a promising photoluminescence imaging technology that offers unique properties, including long luminescence lifetimes, high photostability (non-bleaching and non-blinking), narrow emission bandwidths, large anti-Stokes shifts, low background light compared to the down-conversion biological labels (e.g., organic dye markers and quantum dots) and low toxicity, making them more suitable as medical imaging agents than conventional organic dyes.[11-16] Lanthanide-based UCNPs have been the most commonly used probes in UCL imaging for providing visible or near-infrared emission under continuous-wave excitation at 980 nm. The superior features of lanthanide-UCNPs probes can be readily incorporated with different magnetic, radiopaque, and optical lanthanide ions for multimodality bioimaging contrast agents.[17] In particular, paramagnetic properties of lanthanide ions allow UCNPs to serve as promising MRI contrast agents.[12] However, conventional UCNPs doped by Yb^{3+} ions as sensitizers require excitation light around 980 nm, which risks local temperature increases and substantial overheating inducing unintended cell death and tissue injury, which consequently would restrict practical applications for clinical imaging.[18-21] Recently, considerable efforts have been devoted to the design UCNPs that utilize Nd^{3+} as the sensitizer for alleviation of the overheating effect.[18-24] Furthermore Nd^{3+} has been widely used as components of strong commercial magnet materials (i.e., NdFeB) due to

affordable prices being the second most abundant of the lanthanide series with paramagnetic properties.[25] While Nd^{3+} could be used as both a sensitizer and a MRI contrast agent for the design of a multimodal imaging nano-reporter, no application of Nd^{3+} ions serving as both a sensitizer and a contrast agent to pre-operative diagnosis and intra-operative image-guided cancer therapy has yet been reported.

Herein, we present a targeted Nd^{3+}-doped core-shell UCNP (Nd-CSUCNP) to serve as a multimodal-imaging reporter providing tumor-specific detection, surgical intervention and image-guided surgery for resection of hepatocellular carcinoma (HCC). HCC presents a unique pathophysiology that favors selective delivery of therapeutics and imaging agents to the target malignancies through transcatheter intra-arterial (IA) infusion. This delivery route permits significantly enhanced tumor uptake of infused agents with attendant reduction in systemic toxicity.[26-29] In our study, a multi-modal imaging reporter, Nd-CSUCNP conjugated with HCC tumor specific anti-CD44 monoclonal antibody, was delivered intra-arterially and the *in vivo* feasibility of multimodal diagnostic MR and intraoperative UCL image-guided surgery for HCC resection was demonstrated in orthotopic HCC rat models (Figure 1). This is the first report describing multimodal image-guided surgery via the application of biocompatible nanomaterials integrating MRI and UCL imaging for potential HCC surgical resection applications.

2. Results and Discussion

2.1. Synthesis of Nd^{3+} doped core-shell UCNPs (Nd-CSUCNPs)

Monodisperse nanoparticles ($NaYF_4$:30%Yb^{3+}/1%Nd^{3+}/0.5%Er^{3+}) as a core material were obtained by a thermal decomposition method (Figure 2a).[18, 20] Then, a $NaYF_4$:30%Nd^{3+} shell was coated on the surface of the $NaYF_4$:30%Yb^{3+}/1%Nd^{3+}/0.5%Er^{3+} core through a seed-mediated process.[18, 20] The grown Nd^{3+} shell layer over the inner core increased the diameter of UCNPs without a change in structural and morphological uniformity (Figure 2a (inset)). X-ray diffraction (XRD) patterns of the Nd-CSUCNPs were indexed as the pure hexagonal phase $NaYF_4$ crystal (JCPDS 16-0334) in Figure S1. Using the Scherrer equation, the sizes of the core and the Nd-CSUCNPs were calculated to be 24.7 and 29.9 nm, respectively, consistent with the sizes observed with TEM.

2.2. *In vitro* cytotoxicity and cell-targeting efficiency of biofunctionalized Nd-CSUCNPs

To apply the Nd-CSUCNPs for bio-imaging, the as-synthesized surface of Nd-CSUCNPs were converted into hydrophilic amine-terminated Nd-CSUCNPs via a ligand exchanging process using a biocompatible poly(allyamine) (PAAm)[30] and then the amine-terminated Nd-CSUCNPs were conjugated with anti-CD44 monoclonal antibody using SATA and sulfo-SMCC for HCC tumor targeting. The mean hydrodynamic diameter of amine-terminated Nd-CSUCNPs was 76.03 nm (Figure S2) and zeta potential was 36.5 ± 2.4 mV. The successful conjugation of the anti-CD44 antibody onto the Nd-CSUCNPs was evidenced by observing characteristic bands corresponding to amide groups of antibodies in Fourier transform infrared (FT-IR) spectra (Figure S3). A Zeta potential value of antibody-conjugated Nd-CSUCNPs was 26.4 ± 2.9 mV. The zeta potential of Nd-CSUCNP was slightly decreased by antibody conjugation but the zeta potential value was stably

maintained for 7 days (Figure S4). The amount of bound anti-CD44 antibody was 12 μg of CD44 per 1 mg of Nd-CSUCNPs (Figure S5). Prior to subsequent *in vivo* imaging experiments, cytotoxicity of the PAAm-stabilized Nd-CSUCNPs was evaluated in N1S1 hepatoma cells and Clone-9 liver epithelial cells by an MTT (3-[4, 5-dimethylthiazol-2-yl]-2, 5 diphenyltetrazolium bromide) assay. The resulted viabilities of N1S1 and clone9 were maintained at over 80 % for the tested range up to 400 μg/mL at 24 and 72 hours co-incubation with the PAAm-stabilized Nd-CSUCNPs (Figure S6a). HCC tumor cell targeting of the anti-CD44-Nd-CSUCNPs was investigated with *in vitro* cell studies using N1S1 hepatoma cells. High expression level of the targeted CD44 (transmembrane glycoprotein) receptors on N1S1 (hepatoma) cells (97.3 %) was confirmed with flow-cytometry analysis (Figure S6b). Normal liver cells Clone9 showed low level expression of CD44 (2.1%) (Figure S6b). Conversely, the overexpression of CD44 receptors on the N1S1 hepatoma cells can facilitate recognition by anti-CD44-Nd-CSUCNPs to induce specific targeting of the Nd-CSUCNPs to the hepatic tumors (N1S1).[31, 32] As a matter of fact, when the FITC labeled anti-CD44-Nd-CSUCNPs were incubated with N1S1 hepatoma cells, fluorescence imaging demonstrated green fluorescent signal that confirmed efficient selective binding of anti-CD44-Nd-CSUCNPs (Figure S6c).

2.3. Optical properties of Nd-CSUCNPs

We investigated the optical properties of core and Nd-CSUCNPs using NIR absorption spectroscopy and a wavelength-tunable laser system. As shown in Figure 2a, Nd-CSUCNPs showed multiple NIR absorption bands at around 800 and 865 nm, respectively while Yb^{3+} in the core structure produced an absorption band at *ca* 980 nm. Nd^{3+} is a strong NIR absorber and sensitizer for biological and medical applications for multiple reasons. The absorption cross section of Nd^{3+} at 808 nm is 10 times higher than that of Yb^{3+} at 980 nm (1.2×10^{-19} cm^2 vs. 1.2×10^{-20} cm^2).[18] The use of Nd^{3+} in the 800-865 nm region is expected to avoid biological overheating and auto-fluorescence and increase the penetration (probing) depth, a feature particularly advantageous for *in vivo* imaging. Small doping of Nd^{3+} (1%) in the core prevents the localized harsh quenching by co-doping Nd^{3+} with an activator (i.e. energy back-transfer from the activator to ^4I_J manifolds of Nd^{3+}).[21]

When the excitation laser wavelength was set to NIR range from 785 nm to 815 nm, visible range emission dependent on the excitation wavelength was displayed (Figure 2d). The brightest emissions were found for laser excitation wavelengths at roughly 794 nm to 805 nm (Figure 2d). As we expected, the two intense emission peaks were identical in position to the two strong absorption peaks (Figures 2a and d). The significantly enhanced luminescence observed at 520, 540 and 660 nm (corresponding to characteristic bands of Er^{3+} ($^2H_{11/2}$, $^4S_{3/2}\rightarrow{}^4I_{15/2}$, $^4F_{9/2}\rightarrow{}^4I_{15/2}$) was achieved by Nd^{3+}-dopants (30%) in the shell layer (Figures S6 and S7) of Nd-CSUCNPs. The Nd^{3+} doped shell layer effectively harvested NIR light (around 800 nm wavelength) and enhanced the upconversion emission by separating the surface relevant quenching centers (i.e., defect) and the luminescence centers (i.e., activators) inside the core (Figure S7). As shown in the energy transfer pathway of the synthesized core-shell UCNPs (Figure S8), The Nd^{3+} ions served as the sensitizer to harvest 800 nm photons resulting in a population of the $^4F_{5/2}$ state of Nd^{3+}. The Yb^{3+} ions are used to extract the excitation energy from Nd^{3+} ions through interionic cross-relaxation

and transfer to the Er^{3+} ion activator, which facilitates energy transfer from Nd^{3+} ions to Er^{3+} ions. The phase transfer for the functionalization with PAAm had negligible influence on the luminescence spectrum, as shown strong luminescence at 520, 540 and 660 nm (Figure 2b). The same UCL imaging properties of the UCNPs were also clearly demonstrated in 1:10 diluted whole blood samples (Figure S9).

2.4. Characterization of MR contrast effect of Nd-CSUCNPs

The magnetic properties of the core UCNPs and NIR absorbing Nd-CSUCNPs were investigated using a superconducting quantum interface device (SQUID) magnetometer. The magnetizations of both the triply-doped core/shell structures in the presence or absence of 30% Nd^{3+} doping were proportionally increased with the applied magnetic field indicative of typical paramagnetic behavior. The Nd-CSUCNPs (30% Nd^{3+}-doped shell layer) had higher magnetization than the UCNPs with non-doped shell layer at the same magnetic field strength (Figure S10). Then, MRI T2 contrast effects of Nd-CSUCNPs in 1% agar phantoms were investigated with a 7T MRI system (Figure 2e). T2-weighted contrast effects of the Nd-CSUCNPs were clearly seen within MRI T2 map images. The effective magnetic moments (μ_{eff} = 9.60, 4.50 and 3.62 μ_B of Er^{3+}, Yb^{3+} and Nd^{3+}) of each element in the Nd-CSUCNPs contributed strong MRI T2 contrast effects.[33, 34] Their T2-weighted contrast effects (increasing MR signal loss with increasing UCNPs concentration) were clearly seen within MRI T2 map images. The measured r_2 relaxivity was 1182 $mM^{-1}s^{-1}$ (mM: concentration of lanthanide components) which was 1.7 fold higher than core UCNPs (r_2=682 $mM^{-1}s^{-1}$) (Figure 2c). r_2/r_1 ratio of core UCNPs (r_2/r_1=8886) was also increased to a 2.9-fold higher value (r_2/r_1=25807; r_2= 1182 $mM^{-1}s^{-1}$ and r_1=0.0458 $mM^{-1}S^{-1}$)) for Nd-CSUCNPs (Figure S11). The resultant r_2/r_1 ratio of Nd-CSUCNPs was much higher than Ferumoxytol (r_2/r_1=2019 $mM^{-1}S-1$) which is in clinical trials as MRI T2 contrast agents[35, 36]; these findings suggest that our lanthanide ion-doped UCNPs are efficient as T_2-MRI contrast agents (Figure S11). To date, Ho^{3+}-based UCNPs have been developed for luminescent/MRI T2 dual-modal imaging probes.[33] Although the effective magnetic moments of Ho^{3+} (μ_{eff}=10.60 μ_B)[33, 34] is larger than other lanthanide ions, the doping concentration of Ho^{3+} has been constrained to very low levels (less than 2%) to optimize luminescent intensity. Therefore, the relatively low amount of magnetic materials in the total amount of matrix materials as well as excitation wavelength at 980 nm may limit clinical imaging applications.

2.5. Transcatheter intra-arterial infusion and *in vivo* MRI and UCL imaging of anti-CD44-Nd-CSUCNPs

An orthotopic HCC rat model and transcatheter IA targeted infusion technique were employed to demonstrate *in vivo* multimodal imaging properties and evaluate potential application for image-guided surgical resection of HCC (Figure 1). Prior to *in vivo* multimodal imaging, the undesirable heating effects of Nd-CSUCNPs upon exposure to imaging sources of an 808 nm NIR laser and commonly used 980 nm NIR laser at a power density of 361 mW/cm^2 were compared by monitoring temperature changes in *ex vivo* rat liver tissues. Irradiation with a 980 nm laser demonstrated strong local heating effects and a significant rise (ΔT=+16.3 °C) in temperature after 50 s. In contrast, the temperature increase for the liver tissue irradiated with 808 nm laser was only ΔT=4 °C after the same

exposure duration (Figure S12). To evaluate *in vivo* multimodal imaging properties of anti-CD44-Nd-CSUCNPs, HCC tumor was grown in left hepatic lobe. Transcatheter IA infusion of anti-CD44-Nd-CSUCNPs was successfully performed with X-ray digital subtraction angiographic (DSA) guidance. MRI scans at pre/post IA infusion readily demonstrated detection of the anti-CD44-Nd-CSUCNPs with marked signal reductions within peripheral zones and core of HCC tumors on T2-weighted images (Figure 3a). Then, UCL imaging allowed visualization of the IA infused anti-CD44-Nd-CSUCNPs in the HCC tumor region with NIR 808 nm laser excitation. Significant bright signal from the targeted anti-CD44-Nd-CSUCNPs was observed in the central and peripheral portion of tumor region rather than normal liver parenchymal tissues (Figure 3a, right). These luminescent regions were well correlated with signal reduction within the T2-weighted images (Figure 3a). The MRI and UCL multimodal imaging of UNCPs deposited on tumors could translate to improved removal of neoplastic tissues, especially in the setting of non-anatomical resections, to ultimately reduce the rate of treatment failures due to recurrence.

The biodistribution of targeted anti-CD44-Nd-CSUCNPs after IA infusion were investigated with Yb elemental analysis in each organ with inductively coupled plasma-mass spectrometry (ICP-MS). The highest amount of Nd-CSUCNPs (4.3 μg-Yb/g of tissue) was accumulated within the targeted HCC tumor at 4 h post IA infusion (Figure. 3b). IA infusion of anti-CD44-Nd-CSUCNPs increased targeting efficiency approximately ~5 fold over IV injection and 35% of the targeted anti-CD44-Nd-CSUCNPs was still detected in the tumor region at post 10 days IA injection (Figure 3b and Figure S13). The amount of targeted particles was decreased by reticuloendothelial system (RES) uptake after 3 and 10 days, as shown the increased amounts of particles in kidney and spleen. For *in vivo* toxicity, the current dosage (2 mg) of anti-CD44-Nd-CSUCNPs for MRI and UCL imaging caused no significant toxic effects and histologic changes in the major organs of the HCC rats within 30 days post-injection (Figure 3b). Blood tests also demonstrated no systemic toxicities of anti-CD44-Nd-CSUCNPs (2 mg) with regular level of alanine aminotransferase (ALT), aspartate aminotransferase (AST), bilirubin and albumin in the blood (Figure S14).

2.6. *In vivo* HCC surgical resection guided by multimodal pre-procedural MRI and UCL using IA targeted anti-CD44-Nd-CSUCNPs

Finally, to demonstrate proof-of-concept for multimodal MR/UCL image-guided resection of hepatic malignancies with anti-CD44-Nd-CSUCNPs imaging reporters, HCC tumors in orthotopic N1S1 HCC rats were resected with the guidance of MR imaging and real-time UCL visualization of anti-CD44-Nd-CSUCNPs imaging reporters. Anti-CD44-Nd-CSUCNPs were successfully injected with transcatheter IA procedures as described previously. MRI T2 scan was able to identify the location of tumor region confirmed with targeted anti-CD44-Nd-CSUCNPs on tumors (Figure 4a). Then, under NIR-illumination with a hand-held irradiation source, green luminescence from anti-CD44-Nd-CSUCNPs was co-localized within tumor tissues (Figures 4b and c). Significantly higher UCL intensity (green signal) than the surrounding normal liver tissues was visually observed. Precise burns at these extrema defined the craniocaudal and mediolateral extent of the lesion and a circumferential resection around these areas was performed (Figure 4d) to spare the vast majority of the left lateral lobe. The large remnant lobe was scanned along the margins with

a NIR laser demonstrating no residual anti-CD44-Nd-CSUCNPs in these tissues, suggesting R0 (i.e., curative) resection. This was later confirmed by histopathology, demonstrating the HCC tumor of all suspected tissues detected by UCL imaging and no viable HCC cells in the remnant lobe (Figure 4e). Surgical resections in HCC treatment are definitive and potentially curative interventions. MRI and real-time intraoperative image guidance is expected to refine a surgeons' visual assessment of the surgical bed, reducing the rate of undetected small satellite tumors and extensions of diffuse HCC.

A limitation of the use of UCNP in our study is that real-time NIR-UCL scanning/imaging devices for use in patients. The NIR beam area could broaden by using NIR Light-emitting diode (LED) array platform, which is an integrated circuit of each LED. NIR LED array platform with high power density should be developed for the depth of penetration into tissues. A second limitation is that despite the demonstrated non-toxic effects of our nano-reporters, further long-term toxicity and excretion studies are required prior to future clinical translation.

3. Conclusion

In our studies, Nd^{3+} ions serving as both a sensitizer and a contrast agent in UCNPs were selected for multimodal imaging capability. While a relatively simple HCC tumor model having a single primary tumor was used in this study to demonstrate potential image-guided surgical resection of HCC using antibody conjugated UCNPs and selective IA infusion technique (interventional approach), we believe that our multimodal imaging antibody conjugated Nd-CSUCNPs reporters will serve as an ideal platform for translational into clinical image-guidance strategies with the potential to enhance the tumor detection rates during surgical interventions combined with pre-procedural and intraoperative image-guidance approaches. Further, we anticipate that the incorporation of patient-specific targeting agents with MRI/UCL nano-reporters should lead to superior spatial localization of tumors and provide valuable diagnostic feedback that can assist surgeons to define more optimal surgical margins. As a result, our proposed multimodal Nd-CSUCNPs nano-reporters may ultimately yield an interactive new surgical guidance paradigm.

4. Experimental Section

Chemicals

Yttrium acetate hydrate (99.9%), Ytterbium acetate hydrate (99.9%), neodymium acetate hydrate (99.9%), erbium acetate hydrate (99.9%), sodium hydroxide, ammonium fluoride, 1-octadecene, oleic acid, Poly(allyamine) (PAAm), were all purchased from Sigma-Aldrich.

Synthesis of Nd^{3+} doped core upconversion nanoparticles (CUCNPs)

In a typical synthesis procedure,[18, 20] $NaYF_4$:0.5% Er, 1% Nd, 30% Yb, 1-octadecene (7 mL) and oleic acid (3 mL) were added into the 50 mL flask followed by adding a water (2 mL) containing $Y(CH_3CO_2)_3$, $Yb(CH_3CO_2)_3$, $Er(CH_3CO_2)_3$, and $Nd(CH_3CO_2)_3$ with a total lanthanide amount of 0.4 mmol. Subsequently, the mixture was heated to 150 °C for 1 h and then cooled to room temperature. Later, a methanol solution (6 mL) containing NH_4F (1.6 mmol) and NaOH (1 mmol) was added and the solution stirred at 50 °C for 30 min, followed

by evaporating methanol from the reaction mixture at 100 °C. Upon removal of methanol, the solution was heated to 290 °C and maintained for 1.5 h under a nitrogen flow, then cooled down to room temperature. The resulting nanoparticles were washed with ethanol and methanol several times and finally re-dispersed in cyclohexane.

Synthesis of Nd^{3+} doped core-shell UCNPs (Nd-CSUCNPs)

A $NaYF_4$:Nd shell precursor was prepared by mixing a water (2 mL) containing $Y(CH_3CO_2)_3$, and $Nd(CH_3CO_2)_3$ with a total lanthanide amount of 0.4 mmol, 1-octadecene (7 mL) and oleic acid (3 mL) followed by heating to 150 °C for 1 h and then cooled to room temperature. Later, cyclohexane (2 mL) containing core nanoparticles was added along with a methanol solution (6 mL) containing NH4F (1.6 mmol) and NaOH (1 mmol). The reaction mixture was stirred at 50 °C for 30 min and increased to 100 °C to remove the methanol. Then the solution was heated at 290 °C and maintained for 1.5 h under a nitrogen flow. The resulting nanoparticles were washed with ethanol and methanol several times and re-dispersed in cyclohexane.

Preparation of PAAM-stabilized Nd-CSUCNPs

The ligand exchange process was carried out to transfer as-prepared oleate-stabilized nanoparticle dispersion into hydrophilic ones using PAAM as a ligand. PAAM 20% solution (200 μL) was dispersed in ethanol (10 mL). Cyclohexane (2 mL) containing the UCNPs (5 mg) was mixed with the PAAM solution and stirred vigorously over 24 h at 30 °C. The resulting PAAM-stabilized Nd-CSUCNPs were collected by centrifugation and re-dispersed in water.

Anti-CD44 monoclonal antibody conjugation with Nd-CSUCNPs

PAAM-stabilized Nd-CSUCNPs were bio-functionalized with anti-CD44 monoclonal antibodies. 50 μg of anti-CD44 antibodies were reacted with SATA of 2.54 μg under 0.2 mL of HEPES buffer (10 mM, pH 7.4) for 45 min at room temperature (molar ratio of antibody to SATA is 1:18).[37] After first reaction, 50 uL of hydroxylamine hydrochloride solution (0.5 M) was added to reactant and further incubated for 2 h. Byproduct and un-reacted reagents were removed by dextran desalting column. Concentration of antibody was determined by a micro BCS assay (Thermo Fisher Scientific Inc., IL, USA). To fabricate anti-CD44-nanoparticles, the amine-introduced Nd-CSUCNPs (2 mg) were reacted with 0.2 mg of sulfosuccinimidyl-4-N-maleimidomethyl cyclohexane-1-carboxylate (sulfo-SMCC) under 1 ml of PBS buffer (150 mM, pH 7.2) for 30 min at room temperature. To remove free sulfo-SMCC, the reactant was passed through a dextran desalting column. Finally, thiolated anti-CD44 antibody (25 μg) and maleimide-modified Nd-CSUCNPs (1 mg) were reacted under HEPES buffer (10 mM, pH 7.2) for 24 h at 4 °C. Unreacted antibody was removed by centrifugation (3 times at 15000 rpm, 5 min) with MilliQ water followed by re-suspension in PBS buffer. The anti-CD44 monoclonal antibody conjugated UCNPs were then stored at 4°C.

Characterization

TEM characterization of particle sizes and shapes was performed with a Tecnai Spirit G2 applying an acceleration voltage of 120 keV. Magnetic properties were measured using a SQUID magnetometer (Quantum Design, USA). ATR/FT-IR spectroscopy was performed using a Bruker Vertex 70 spectrometer equipped with an attenuated total reflection accessory over the frequency range 4000-700 cm^{-1}. Dynamic light scattering (DLS) and zeta potential distribution measurements were performed using a Malvern Zetasizer Nano ZS (Malvern Instruments Ltd., UK). Upconversion emission spectra were obtained using a USB spectrometer (Ocean Optics USB2000+) and a wavelength-tunable Ti-Sapphire laser (Coherent Indigo-S) as excitation source in the 785-815 nm regions. Laser power was maintained at 200 mW. The emission from the laser-irradiated sample was collected at 90° configuration by a collimating lens, a 750 nm IR cutoff filter, and an optical fiber connected to the spectrometer.

Cell culture

N1S1 rat hepatoma cell line and Clone9 epithelial cell line (ATCC, CRL-1603, Manassas, VA, USA) were obtained and cultured in their respective Dulbecco's Modified Eagle's Medium (DMEM, ATCC, Manassas, VA, USA) and F-12K medium (ATCC, Manassas, VA, USA) supplemented with 10% fetal bovine serum (Sigma-Aldrich, MO, USA) and 0.1% gentamycin (Sigma-Aldrich, MO, USA). For orthotopic HCC rat models, the viability of the N1S1 rat hepatoma cells was tested with Trypan blue staining (confirming > 90% cell viability for each tumor implantation procedure).

In vitro cytotoxicity of UCNPs

Cytotoxicity of the Nd-CSUCNPs was evaluated in N1S1 hepatoma cell line and Clone 9 liver cell line (ATCC, CRL-1601, Manassas, VA, USA) by MTT assay. Cells from the exponential phase of the culture were harvested and diluted to a cell density of about 2×10^4 per mL. 100 uL of the cell suspension was added to 180 ul of medium in each well of a 96-well plate, incubated at 37 °C, 5% CO_2 and 95% air for 1 day. A 100 uL solution consisting of different amounts of Nd-CSUCNPs was then added to the respective wells and incubated for specific periods of time. Control studies were conducted by exposing cells to normal saline. Exposure time was 24 and 72 h. Treated cells were then rinsed with PBS before 20 uL of PBS containing 5 mg/ml of MTT was added prior to incubation for another 4 h. This was followed by the addition of 150 uL of DMSO and plate agitation for 10 min. The optical density (OD) of the contents in each well was then measured at 570 nm using a bioassay reader (SpectraMax M5, Molecular Devices, CA, USA). OD measurements were repeated in triplicate. Cell viability for each sample was calculated as the ratio between OD measurements within control and treatment wells (%viability = ($OD_{treatment}$/ $OD_{control}$)*100). Significant differences were determined using the Student's t-test where differences were considered significant for p-values < 0.05.

In vitro cell targeting

To measure CD44 expression level on N1S1 cells, cells were treated with FITC-anti-CD44 monoclonal antibody for 24 h and analyzed with fluorescence-activated cell sorting (FACS)

(Becton Dickinson LSRFortessa flow cytometer). The percentage of FITC-anti-CD44 monoclonal antibody was determined. Data were collected using CellQuest software (BD Biosciences) and analyzed using FCS Express (De Novo Software). To study gross cellular interactions of the anti-CD44-Nd-CSUCNPs, FITC labeled anti-CD44-Nd-CSUCNPs were prepared and 3×10^4 N1S1 cells were seeded onto 24 wells and incubated for 24h at 37°C in 5% CO_2 prior to addition of the nanoparticles. The N1S1 cells were exposure to these particles for 24 h. Next, the exposure medium was removed and all samples washed 3 times with PBS and fixed for 20 min in 4% neutral buffered formalin solution. A fluorescent microscope (Cytation3, Biotek, USA) was then used to capture images of the cellular localization of the fluorescently labeled anti-CD44-Nd-CSUCNPs.

Characterization of MR Relaxivity Properties of Nd-CSUCNPs

r2 and r1 relaxivities for the Nd-CSUCNPs were determined using a 7 Tesla MRI scanner (BioSpec, Bruker, Billerica, MA, USA). Imaging phantoms were prepared by diluting samples in 1% agarose at various concentrations of UCNPs. The atomic Yb concentrations of the stock solutions were determined using Inductively Coupled Plasma Spectroscopy (ICP-MS, Perkin Elmer, Waltham, MA, USA) and MRI signal changes were measured for increasing concentrations of the Nd-CSUCNPs. For T2 measurement, a Carr-Purcell-Meiboom-Gill (CPMG) sequence of 6 echoes was used with TR = 1024ms and TE = 10.5~63 ms with an echo interval of 10.5 ms. The T2 values were calculated using a least squares single exponential fitting model (pixel by pixel) and then averaging over the ROIs. For each concentration, we performed a linear fit between R2 relaxation value and particle concentration with corresponding slope thus providing r2 relaxivity estimates. T1 was measured using a spin-echo sequence with different repetition time (TRs=100~2500ms) and an echo time (TE=2.09ms). T1 measurements were performed using a nonlinear fit to changes in the mean signal intensity of each sample as a function of TR. The r1 relaxivity values were determined through the curve fitting of R1 relaxation time (s^{-1}) versus the lanthanide Yb component concentration (mM).

Orthotopic Rat Hepatoma Model

Animal studies were performed with approval from Institutional Animal Care and Use Committee (IACUC). N1S1 hepatoma cells were implanted in the left lateral liver lobe during mini-laparotomy procedures in 16 male Sprague Dawley rats. Briefly, rats were anesthetized with isoflurane (mixture of 5% isoflurane and oxygen at 3 L/min). A mini-laparotomy was performed and left hepatic lobe exposed. 1×10^6 N1S1 hepatoma cells were injected in the left lateral lobe and surgical site closed in 2-layers. Tumors were allowed to grow for 7 days to reach a size typically >5mm in diameter while observing animal daily for any signs of distress.

Hepatic Intra-arterial Transcatheter Targeting of anti-CD44-Nd-CSUCNPs

7 days after implantation, animals were scanned with MRI to confirm tumor growth. T2 weighted images were collected using a gradient-echo sequence (details in next imaging section). The following steps were used to invasively catheterize the left hepatic artery (LHA) for selective infusion of the anti-CD44-Nd-CSUCNPs in each animal.[26, 27] First, rats were anesthetized with an isoflurane induction. After laparotomy, a cotton-tipped

applicator was used to expose the common hepatic artery (CHA), proper hepatic artery (PHA), and gastroduodenal artery (GDA). A micro bulldog clamp (World Precision Instruments, Sarasota, FL) was placed on the CHA to prevent bleeding during catheterization. 4-0 Vetacryl absorbable polyglycolic acid suture (Webster Veterinary, Devens, MA) was then used to ligate the GDA distally to control retrograde bleeding during catheterization. Next, a 24G SurFlash polyurethane catheter (Terumo Medical Co., Somerset, NJ) was inserted into the GDA, advanced into the PHA and then distally into the LHA. X-ray digital subtraction angiographic (DSA) was used to confirm catheter placement in common branch of PHA using iodinated contrast (Omnipaque, Amersham). After selective catheterization, 0.1 mL of heparin was infused before infusing the Nd-CSUCNPs (2 mg in 200 uL); each infusion was followed by a 0.2 mL saline flush. The catheter was then withdrawn, and a 3-0 suture used to permanently ligate the GDA above the insertion position. Finally, abdomen was closed using two-layer technique. The animals were then moved to the MRI scanner located adjacent to the surgical suite.

In Vivo multimodal UCL and MR imaging of IA targeted anti-CD44-Nd-CSUCNPs in HCC rat model

For n=4 animals, after IA targeting of anti-CD44-Nd-CSUCNPs, UCL imaging was performed with an 808 nm laser with a power density of 361 mW/cm^2 as the excited source, digital single-lens reflex camera (Canon, T3) and 52mm UV-IR cut filter (Neewer Global, USA). A laser protective goggle (Kentek Corporation, Pittsfield, NH, USA) with minimal safety rating of OD6+ (800-818 nm) was worn to prevent eye injuries during UCL imaging. Then, T2-weighted images were collected again to confirm the distribution of anti-CD44-Nd-CSUCNPs. The rats were anesthetized with isoflurane (mixture of 5% isoflurane and oxygen at 2 L/min) during imaging. MR scans were performed in the coronal orientation using a gradient-echo sequence with following parameters: TR/TE=1,300/7.2 ms, 0.7 mm slice thickness, FOV 71 × 85mm, 216 × 256 matrix, respiratory triggering with MRI-compatible small animal gating system (Model 1025, SA Instruments, Stony Brook, NY). UCL images were analyzed with the aid of image processing software (Image J).

Biodistribution and systemic toxicity of anti-CD44-Nd-CSUCNPs

Biodistribution of the anti-CD44-Nd-CSUCNPs was investigated in 6 rats after hepatic intra-arterial administration. The rats were then euthanized at 4 hours and 10-day time points (each group n=3). For an additional control group (n=3), anti-CD44-Nd-CSUCNPs (2 mg in 200 uL) was injected intravenously for comparison to resulting IA distributions. Major organs (heart, liver, spleen, lung, and kidney) were collected and weighed. Then the atomic Yb concentrations of all the tissues were determined using Inductively Coupled Plasma Spectroscopy (ICP-MS, Perkin Elmer, Waltham, MA, USA). To evaluate *in vivo* systemic toxicity of anti-CD44-UCNPs, anti-CD44-Nd-CSUCNPs (2 mg in 200 uL) were injected intravenously. Then, whole blood from the right ventricle was collected at 1 and 3 days, and centrifuged at 8000rpm for 5min in a green top tube with heparinized plasma sent for biochemistry to assess total bilirubin, albumin, ALP, and ALT.

Histology

Each rat was euthanized after catheterization and imaging procedures. HCC specimens were sliced at 2 mm intervals; these slices were sectioned into 5 um-thick sections for hematoxylin and eosin (H&E) staining to identify organ-specific toxicity of Nd-CSUCNPs and positions of HCC tissues. All slides were digitized at ×200 optical magnification using a TissueFAXS microscope (TissueGnostics GmbH, Vienna, Austria). Post-processing was performed using the HistoQuest software package (TissueGnostics GmbH).

In Vivo multimodal image-guided surgical resection of HCC using targeted anti-CD44-Nd-CSUCNPs

To demonstrate proof-of-concept for multimodal image-guided resection of hepatic malignancy with UCNPs, an orthotopic N1-S1 rodent model of HCC was generated in the Sprague-Dawley rat (n=3) with confirmation of 0.6~1 cm tumor after 7 days on MRI at 7 Tesla. Anti-CD44-Nd-CSUCNPs (2 mg in 200 uL) were injected via intra-arterial administration. After 1 hr, the rat was scanned with MRI to confirm tumor targeting with IA-injected Nd-CSUCNPs and NIR luminescent imaging (808nm laser) of the targeted Nd-CSUCNPs was performed to guide hepatic resection. The luminescent regions were resected with a high temperature cautery unit (2000 °F loop tip, Change-A-Tip, AARon medical industry, USA) attached on NIR laser probe. After resection, the remnant left lateral lobe and tumor naïve right median lobe (as a control) were imaged with NIR laser to confirm the resection of tumors and the resected tissues were fixed in 10% formalin for histopathological analysis.

Supplementary Material

Refer to Web version on PubMed Central for supplementary material.

Acknowledgements

This work was supported by Basic Research Grant from ACS (American Cancer Society, ACS 279148) and by four grants R01CA141047, R21CA173491, R21EB017986 and R21CA185274 from the National Cancer Institute and National Institute of Biomedical Imaging and Bioengineering. This work was supported by the Center for Translational Imaging at Northwestern University. Metal analysis was performed at the Northwestern University Quantitative Bio-element Imaging Center generously supported by NASA Ames Research Center Grant NNA04CC36G. Use of the Center for Nanoscale Materials, an Office of Science user facility, was supported by the U. S. Department of Energy, Office of Science, Office of Basic Energy Sciences, under Contract No. DE-AC02-06CH11357. J.L. acknowledges the Director's Postdoctoral Fellowship from Argonne National Laboratory. The authors thank V. Novosad (Materials Science Division, Argonne) for performing magnetic characterization and useful discussions.

References

1. Jung KH, Lee KH. Molecular imaging in the era of personalized medicine. J Pathol Transl Med. 2015; 49(1):5–12. [PubMed: 25812652]
2. Locke JA, Dal Pra A, Supiot S, Warde P, Bristow RG. Synergistic action of image-guided radiotherapy and androgen deprivation therapy. Nat Rev Urol. 2015; 12(4):193–204. [PubMed: 25800395]
3. Kim DH, Larson AC. Deoxycholate bile acid directed synthesis of branched Au nanostructures for near infrared photothermal ablation. Biomaterials. 2015; 56:154–64. [PubMed: 25934288]
4. Dupuy, DE.; Fong, Y.; McMullen, WN. Image-Guided Cancer Therapy. Springer; New York: 2013.

5. Bouvet M, Hoffman RM. Glowing Tumors Make for Better Detection and Resection. Sci Transl Med. 2011; 3(110)
6. Nguyen QT, Tsien RY. Fluorescence-guided surgery with live molecular navigation - a new cutting edge. Nat Rev Cancer. 2013; 13(9):653–662. [PubMed: 23924645]
7. van Dam GM, Themelis G, Crane LMA, Harlaar NJ, Pleijhuis RG, Kelder W, Sarantopoulos A, de Jong JS, Arts HJG, van der Zee AGJ, Bart J, Low PS, Ntziachristos V. Intraoperative tumor-specific fluorescence imaging in ovarian cancer by folate receptor-alpha targeting: first in-human results. Nature medicine. 2011; 17(10):1315–U202.
8. Vahrmeijer AL, Hutteman M, van der Vorst JR, van de Velde CJH, Frangioni JV. Image-guided cancer surgery using near-infrared fluorescence. Nature Reviews Clinical Oncology. 2013; 10(9): 507–518.
9. Wada H, Hyun H, Vargas C, Gravier J, Park G, Gioux S, Frangioni JV, Henary M, Choi HS. Pancreas-targeted NIR fluorophores for dual-channel image-guided abdominal surgery. Theranostics. 2015; 5(1):1–11. [PubMed: 25553094]
10. Chi C, Du Y, Ye J, Kou D, Qiu J, Wang J, Tian J, Chen X. Intraoperative imaging-guided cancer surgery: from current fluorescence molecular imaging methods to future multi-modality imaging technology. Theranostics. 2014; 4(11):1072–84. [PubMed: 25250092]
11. Zhou L, Wang R, Yao C, Li XM, Wang CL, Zhang XY, Xu CJ, Zeng AJ, Zhao DY, Zhang F. Single-band upconversion nanoprobes for multiplexed simultaneous in situ molecular mapping of cancer biomarkers. Nat Commun. 2015; 6
12. Il Park Y, Lee KT, Suh YD, Hyeon T. Upconverting nanoparticles: a versatile platform for wide-field two-photon microscopy and multi-modal in vivo imaging. Chem Soc Rev. 2015; 44(6):1302–1317. [PubMed: 25042637]
13. Lee JS, Nam DH, Kuk SK, Park CB. Near- Infrared- Light- Driven Artificial Photosynthesis by Nanobiocatalytic Assemblies. Chem-Eur J. 2014; 20(13):3584–3588. [PubMed: 24615772]
14. Chen GY, Qju HL, Prasad PN, Chen XY. Upconversion Nanoparticles: Design, Nanochemistry, and Applications in Theranostics. Chem Rev. 2014; 114(10):5161–5214. [PubMed: 24605868]
15. Zhou B, Shi B, Jin D, Liu X. Controlling upconversion nanocrystals for emerging applications. Nat Nanotechnol. 2015; 10(11):924–36. [PubMed: 26530022]
16. Ai X, Ho CJ, Aw J, Attia AB, Mu J, Wang Y, Wang X, Wang Y, Liu X, Chen H, Gao M, Chen X, Yeow EK, Liu G, Olivo M, Xing B. In vivo covalent cross-linking of photon-converted rare-earth nanostructures for tumour localization and theranostics. Nat Commun. 2016; 7:10432. [PubMed: 26786559]
17. Zhou J, Yu MX, Sun Y, Zhang XZ, Zhu XJ, Wu ZH, Wu DM, Li FY. Fluorine-18-labeled Gd3+/Yb3+/Er3+ co-doped NaYF4 nanophosphors for multimodality PET/MR/UCL imaging. Biomaterials. 2011; 32(4):1148–1156. [PubMed: 20965563]
18. Wang YF, Liu GY, Sun LD, Xiao JW, Zhou JC, Yan CH. Nd3+-Sensitized Upconversion Nanophosphors: Efficient In Vivo Bioimaging Probes with Minimized Heating Effect. Acs Nano. 2013; 7(8):7200–7206. [PubMed: 23869772]
19. Li XM, Wang R, Zhang F, Zhou L, Shen DK, Yao C, Zhao DY. Nd3+ Sensitized Up/Down Converting Dual-Mode Nanomaterials for Efficient In-vitro and In-vivo Bioimaging Excited at 800 nm. Sci Rep-Uk. 2013; 3
20. Xie XJ, Gao NY, Deng RR, Sun Q, Xu QH, Liu XG. Mechanistic Investigation of Photon Upconversion in Nd3+-Sensitized Core-Shell Nanoparticles. J Am Chem Soc. 2013; 135(34): 12608–12611. [PubMed: 23947580]
21. Zhong YT, Tian G, Gu ZJ, Yang YJ, Gu L, Zhao YL, Ma Y, Yao JN. Elimination of Photon Quenching by a Transition Layer to Fabricate a Quenching-Shield Sandwich Structure for 800 nm Excited Upconversion Luminescence of Nd3+ Sensitized Nanoparticles. Advanced Materials. 2014; 26(18):2831–2837. [PubMed: 24338994]
22. Ju Q, Chen X, Ai FJ, Peng DF, Lin XD, Kong W, Shi P, Zhu GY, Wang F. An upconversion nanoprobe operating in the first biological window. J Mater Chem B. 2015; 3(17):3548–3555.
23. Wen HL, Zhu H, Chen X, Hung TF, Wang BL, Zhu GY, Yu SF, Wang F. Upconverting Near-Infrared Light through Energy Management in Core-Shell-Shell Nanoparticles. Angew Chem Int Edit. 2013; 52(50):13419–13423.

24. Zhang X, Ai F, Sun T, Wang F, Zhu G. Multimodal Upconversion Nanoplatform with a Mitochondria-Targeted Property for Improved Photodynamic Therapy of Cancer Cells. Inorg Chem. 2016; 55(8):3872–80. [PubMed: 27049165]
25. Hou YH, Huang YL, Liu ZW, Zeng DC, Ma SC, Zhong ZC. Hot deformed anisotropic nanocrystalline NdFeB based magnets prepared from spark plasma sintered melt spun powders. Mater Sci Eng B-Adv. 2013; 178(15):990–997.
26. Kim DH, Chen J, Omary RA, Larson AC. MRI visible drug eluting magnetic microspheres for transcatheter intra-arterial delivery to liver tumors. Theranostics. 2015; 5(5):477–88. [PubMed: 25767615]
27. Chen J, Sheu AY, Li W, Zhang Z, Kim DH, Lewandowski RJ, Omary RA, Shea LD, Larson AC. Poly(lactide-co-glycolide) microspheres for MRI-monitored transcatheter delivery of sorafenib to liver tumors. J Control Release. 2014; 184:10–7. [PubMed: 24727059]
28. Kim DH, Choy T, Huang S, Green RM, Omary RA, Larson AC. Microfluidic fabrication of 6-methoxyethylamino numonafide-eluting magnetic microspheres. Acta biomaterialia. 2014; 10(2): 742–50. [PubMed: 24161384]
29. Chen J, White SB, Harris KR, Li W, Yap JW, Kim DH, Lewandowski RJ, Shea LD, Larson AC. Poly(lactide-co-glycolide) microspheres for MRI-monitored delivery of sorafenib in a rabbit VX2 model. Biomaterials. 2015; 61:299–306. [PubMed: 26022791]
30. Wang YH, Wang HG, Liu DP, Song SY, Wang X, Zhang HJ. Graphene oxide covalently grafted upconversion nanoparticles for combined NIR mediated imaging and photothermal/photodynamic cancer therapy. Biomaterials. 2013; 34(31):7715–7724. [PubMed: 23859660]
31. Hou Y, Zou Q, Ge R, Shen F, Wang Y. The critical role of CD133(+)CD44(+/high) tumor cells in hematogenous metastasis of liver cancers. Cell research. 2012; 22(1):259–72. [PubMed: 21862973]
32. Qhattal HSS, Liu XL. Characterization of CD44-Mediated Cancer Cell Uptake and Intracellular Distribution of Hyaluronan-Grafted Liposomes. Mol Pharmaceut. 2011; 8(4):1233–1246.
33. Ni DL, Bu WB, Zhang SJ, Zheng XP, Li M, Xing HY, Xiao QF, Liu YY, Hua YQ, Zhou LP, Peng WJ, Zhao KL, Shi JL. Single Ho3+-Doped Upconversion Nanoparticles for High-Performance T-2-Weighted Brain Tumor Diagnosis and MR/UCL/CT Multimodal Imaging. Advanced Functional Materials. 2014; 24(42):6613–6620.
34. Ferenc W, Sadowski P, Cristovao B, Sarzynski J. Investigation of Some Physicochemical Properties of 4-Nitrocinnamates of Lanthanides(Iii). Journal of the Chilean Chemical Society. 2013; 58(2): 1753–1758.
35. Thu MS, Bryant LH, Coppola T, Jordan EK, Budde MD, Lewis BK, Chaudhry A, Ren J, Varma NR, Arbab AS, Frank JA. Self-assembling nanocomplexes by combining ferumoxytol, heparin and protamine for cell tracking by magnetic resonance imaging. Nat Med. 2012; 18(3):463–7. [PubMed: 22366951]
36. Bullivant JP, Zhao S, Willenberg BJ, Kozissnik B, Batich CD, Dobson J. Materials characterization of Feraheme/ferumoxytol and preliminary evaluation of its potential for magnetic fluid hyperthermia. Int J Mol Sci. 2013; 14(9):17501–10. [PubMed: 24065092]
37. Min H, Jo SM, Kim HS. Efficient capture and simple quantification of circulating tumor cells using quantum dots and magnetic beads. Small. 2015; 11(21):2536–42. [PubMed: 25630488]

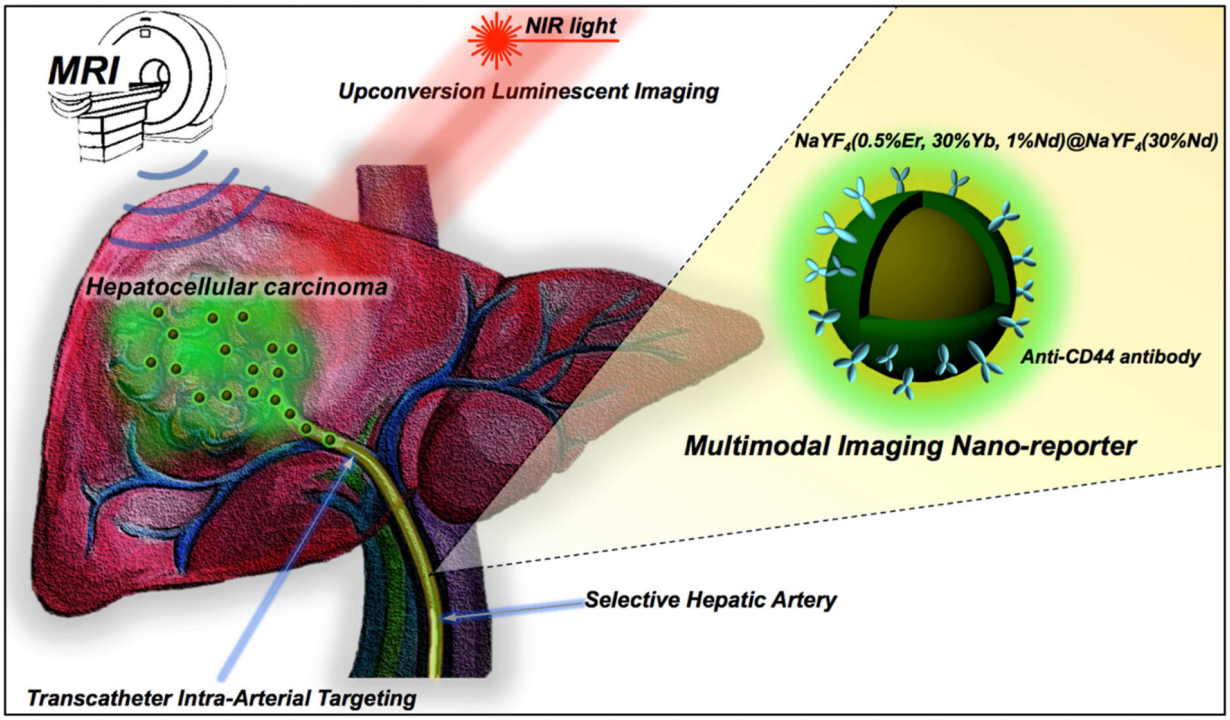

Figure 1.

Schematic of multimodal MR/Upconversion luminescent imaging of HCC tumor using transcatheter hepatic intra-arterial (IA) targeted anti-CD44-Nd-CSUCNPs. Multi-modal imaging reporters, Nd-CSUCNPs conjugated with an anti-CD44 monoclonal antibody, were delivered intra-arterially for the sensitive and rapid detection of HCC in orthotopic HCC rat models. IA delivery of multi-modality Nd-CSUCNPs conjugated with specific tumor targeting molecules facilitates rapid and selective targeting of Nd-CSUCNPs to HCC, providing strong image-contrast between the tumors and normal hepatic tissue. Next, the feasibility of multimodal diagnostic MR and intraoperative UCL image-guided surgery for HCC resection was demonstrated.

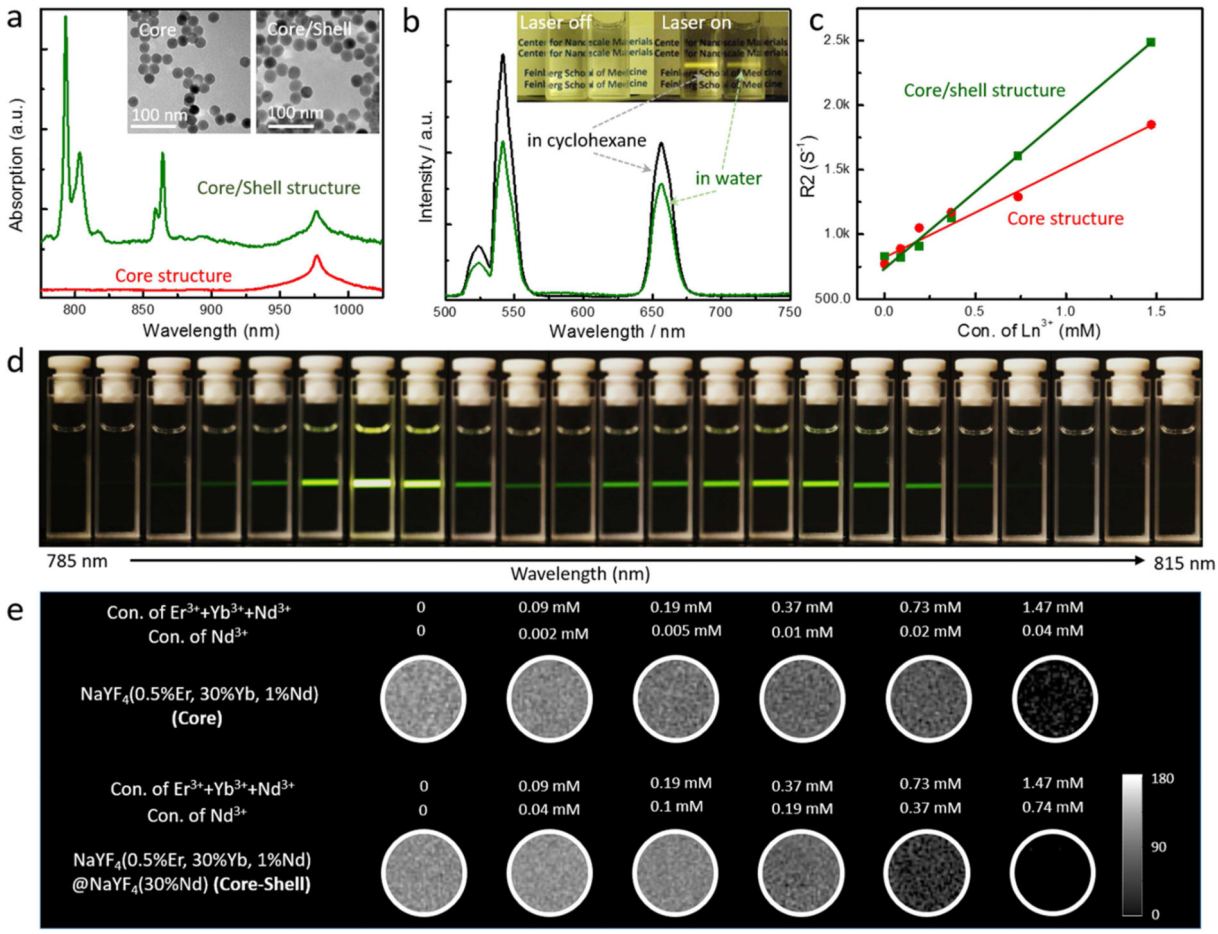

Figure 2.

(a) Near-IR absorption spectra and TEM images of $NaYF_4$:30%Yb/1%Nd/0.5%Er (core) and $NaYF_4$:30%Yb/1%Nd/0.5%Er@NaYF4:30%Nd (core/shell) nanoparticles showing monodispersed size distribution and strong NIR (around 800 nm) absorption of Nd-CSUCNPs. (b) Photographs and upconversion emission spectra for bare Nd-CSUCNPs in cyclohexane and PAAm-stabilized Nd-CSUCNPs in water. The spectra were recorded under excitation by a 796.4 nm laser at power of 20 mW. (d) Emission photographs of $NaYF_4$:30%Yb/1%Nd/0.5%Er@NaYF4:30%Nd (Nd-CSUNCPs) colloidal solution as a function of excitation wavelength when the excitation laser wavelength changed from 785 nm to 815 nm using uniform step size of ~1.3 nm. The brightest emissions were found for laser excitation wavelengths at roughly 794 nm to 805 nm. (c, e) T2 map images and R2 value plots of agarose phantoms containing different concentration of core ($NaYF_4$:30%Yb/ 1%Nd/0.5%Er) and core-shell ($NaYF_4$:30%Yb/1%Nd/ 0.5%Er@NaYF4: 30%Nd) structure UCNPs. UCNPs measured from images of phantoms containing 0-1.5 mM of Ln^{3+} components in UCNPs; the strong linear correlation was observed between R2 and UCNP concentration.

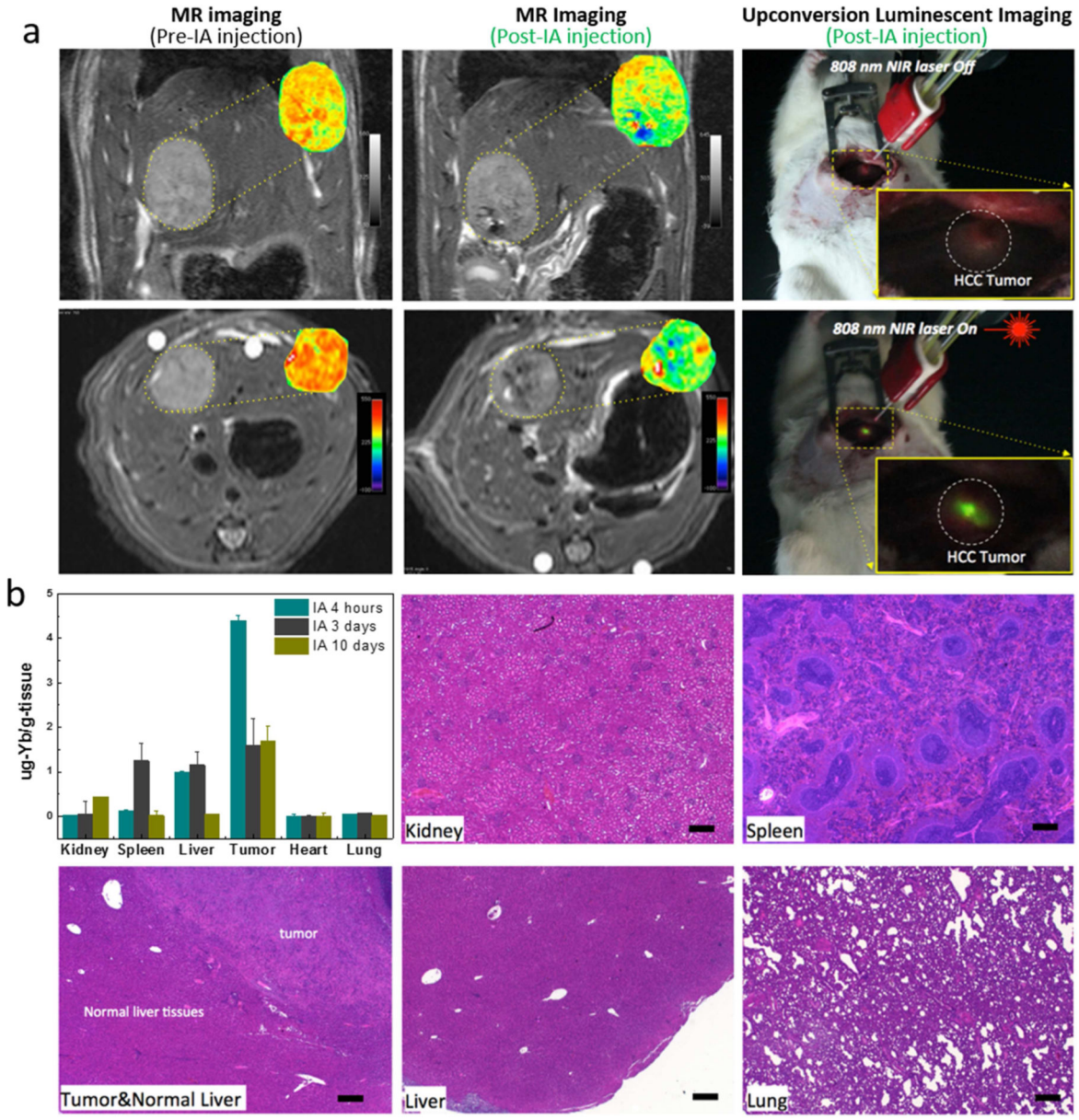

Figure 3.

(a) T2-weighted MR images acquired before and after catheter-directed hepatic IA anti-CD44-Nd-CSUCNP infusion and T2 maps (insets) of HCC tumor regions; (right) intraoperative upconversion luminescent imaging of anti-CD44-Nd-CSUCNP imaging reporters was also performed after IA transcatheter infusion. (b) Biodistribution of Nd-CSUCNPs following IA catheter-directed infusion (4 h, 3 days and 10 days follow-up intervals) and histological analysis of primary organs indicating no histologic changes in these rats 30 days after IA infusion of the anti-CD44-Nd-CSUCNP imaging reporters (scale bars=100 um). Retention of Nd-CSUCNPs in HCC tumor by IA infusion was still observed at 10 days post infusion.

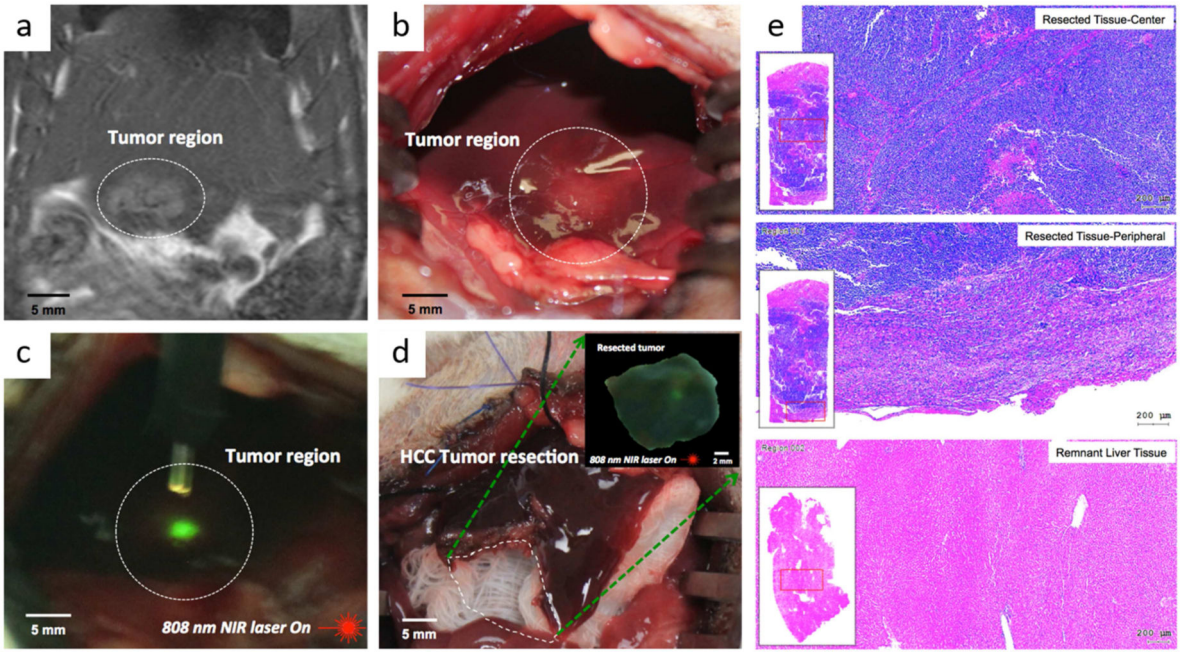

Figure 4.

Multimodal image-guided surgical resection of HCC using IA targeted anti-CD44-Nd-CSUCNP imaging reporters, (a) MR T2 weighted images of rats after IA delivery confirming HCC detection of anti-CD44-Nd-CSUCNP imaging reporters, (b) digital imaging of HCC lesion, (c) detection of HCC with UCL imaging of IA targeted anti-CD44-Nd-CSUCNPs and NIR light (808 nm), (d) an image of liver after image-guided hepatic electro-cauterization resection, (inset) UCL imaging of resected HCC tissue with NIR light (808 nm), (e) representative H&E histologic images of resected tissues (center and peripheral tissues) with multimodal image guidance using anti-CD44-Nd-CSUCNP imaging reporters and remnant liver tissues.